

A Horizontal-winding Multi-permeability Distributed Air-gap Inductor

Laili Wang*, Yunqing Pei[#], Xu Yang[#], Zhaoan Wang[#], Yanfei Liu*

*Department of Electrical and Computer Engineering
Queen's University
Kingston, Canada
l.l.wang@queensu.ca, yanfei.liu@queensu.ca

[#]Department of Electrical Engineering
Xi'an Jiaotong University
Xi'an, China
peiyq@mail.xjtu.edu.cn

Abstract— Distributed air-gap inductors have the advantage of reducing winding loss in high switching frequency DC/DC converters. However, they also have the disadvantage of uneven distribution of flux density, which inevitably leads to the incomplete utilization of magnetic material. This paper proposes a horizontal-winding multi-permeability distributed air-gap inductor structure to increase inductance without the increase of inductor volume. To evaluate the proposed method, a two-permeability inductor together with a single permeability inductor is fabricated. The measured results show the two-permeability inductor has higher inductance than the single-permeability one, especially at light load. Both inductors are tested in a 12V input, 1.6V output DC/DC converter to show their performance. The results show the two-permeability inductor could further improve light load efficiency of high frequency DC/DC converters.

I. INTRODUCTION

The design of inductors used in high frequency DC/DC converters has become very popular in past few decades because it plays an important role in increasing the power density and in improving the efficiency. In conventional high frequency DC/DC converters, the inductors are usually constructed with high permeability commercial magnetic cores and copper wires. For these inductors, air-gaps are needed to guarantee that the magnetic cores do not become saturated. However, the leakage flux from the air-gap will also cause high winding loss, resulting in a reduction of the efficiency [1]. With the purpose of reducing winding loss caused by the air gap, quasi distributed air gap [2-5] and distributed air gap [6-20] techniques are proposed. They are shown in Fig. 1. Among these inductors, the low temperature co-fired ceramic (LTCC) inductors have been proven to have many advantages, such as better system integration, greater loss reduction and easier fabrication [8-20]. Although the LTCC technology has been seen as a promising technology for passive integration, the present LTCC inductors fabricated with low permeability magnetic materials still have the disadvantage of uneven distributing flux density in the

magnetic cores. For inductors designed with high permeability magnetic cores, the flux density in the core can be seen as

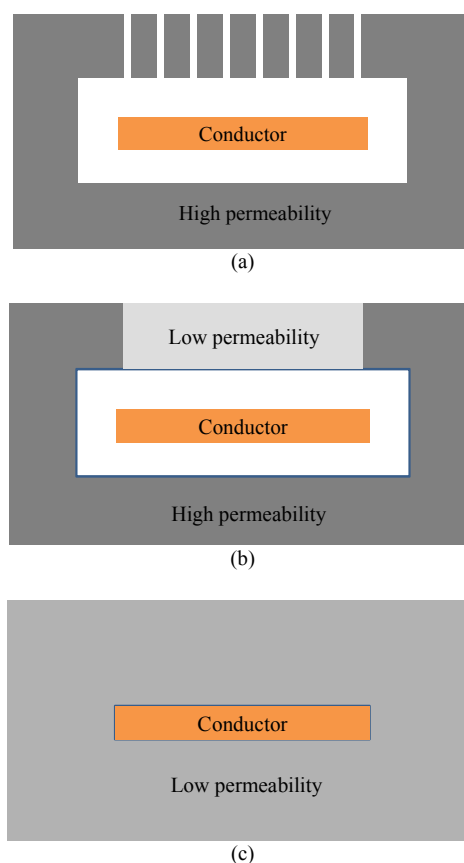


Figure 1. Cross-section view of quasi distributed air gap inductor and distributed air gap inductor. (a) Quasi distributed air gap. (b) Distributed air gap inductor based on conventional high permeability magnetic cores. (c) Distributed air gap inductor based on LTCC or thin film technology

uniform, however, for low permeability distributed air-gap magnetic cores, the flux density in the magnetic cores can no longer be seen as uniform. It will vary according to equivalent magnetic resistance along the flux path. This inevitably makes the magnetic material not fully utilized. Fig. 2 roughly illustrates the flux density distribution in a planar magnetic core with the increase of current. The cross-section of the magnetic core is divided into three regions. At light load, the magnetic material of Region I has higher flux density while that of Region II and Region III have a lower flux density. At intermediate load, the magnetic material of Region I and Region II has higher flux density, but the flux density in Region III is still very low. At full load, Region II and Region III have a higher flux density, but the magnetic material of Region I has become saturated. It can be seen that the magnetic core could not be utilized effectively, especially at light load condition. To make the flux density in the magnetic core distribute more evenly and increase the inductance, multi-permeability inductors are proposed in this paper. Section II of this paper describes the principle of multi-permeability inductors, Section III demonstrates the design of a horizontal winding multi-permeability distributed air-gap inductor based on simulation. Section IV presents the experimental results of a fabricated two permeability inductor as well as a single permeability inductor. Characteristics of the inductor prototypes are measured, and the inductors are evaluated in a DC/DC converter for comparison. Section V is the conclusion.

II. PRINCIPLE OF MULTI-PERMEABILITY INDUCTOR

This section will introduce the principle and advantages of the multi-permeability distributed air-gap inductors. Distributed air-gap inductors could be generally classified into two kinds. One is toroidal inductors, the other one is planar inductors. For the purpose of simplicity, this paper only focus on one turn inductors based on which multiple turns inductors could be easily designed. Fig. 3 shows the structures of the inductors. Their cross-section areas are shown in Fig. 4. Generally, the flux density in the single permeability magnetic core could be expressed by (1)

$$B_r = \frac{\mu_r \mu_0 I}{l_r} \quad (1)$$

Where l_r is the length of magnetic path, B_r is the corresponding flux density along the path, μ_0 is the permeability of air, μ_r is the relative permeability of the magnetic material.

From the inner surface to the outer surface of the magnetic core, l_r gradually increases and B_r thus gradually decreases, which will cause the uneven distribution of flux density. Fig. 5 shows the flux density distribution of the two magnetic cores under 20A excitation. Uneven flux density distribution is observed. When the flux density close to the conductor reaches its peak value, the flux density which is far away from the conductor is still very low. Therefore, the magnetic core could be fully utilized only when every point of the magnetic core reaches the peak flux density B_{max} simultaneously. By increasing the relative permeability of the magnetic material

continuously from the inner surface to the outer surface of the

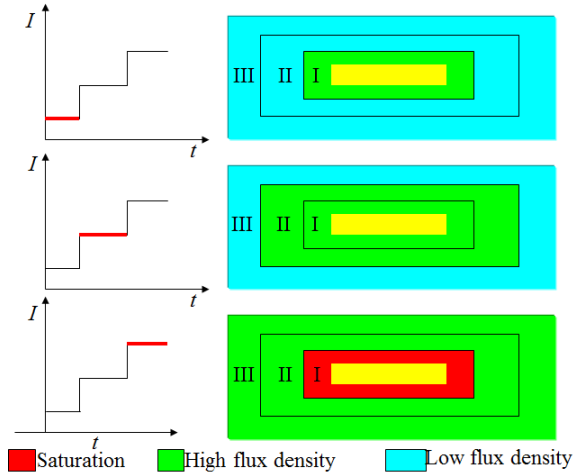


Figure 2. Flux density distribution in a single permeability inductor.

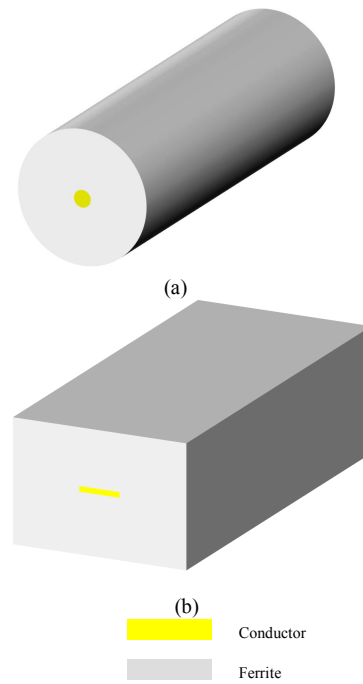


Figure 3. One turn distributed-air gap inductors. (a) Toroidal inductor. (b) Planar inductor.

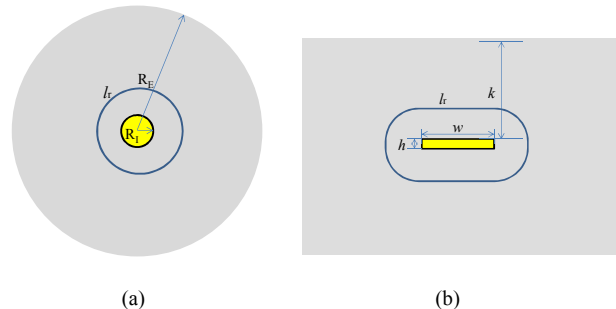
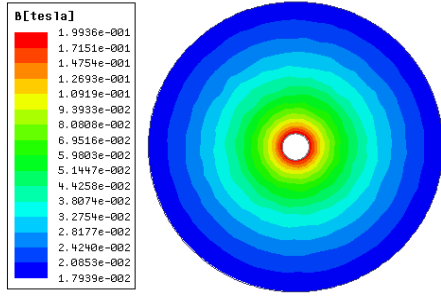
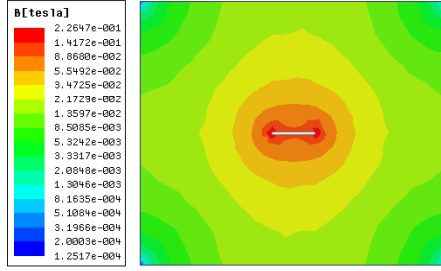


Figure 4. Cross-section views of single permeability inductor. (a) Circular. (b) Square.



(a)



(b)

Figure 5. Flux density distribution in single permeability distributed air gap inductors. (a) Circular. (b) Square.

magnetic core according to (2), this goal could be achieved. The structures of the continuously changing permeability magnetic cores are shown in Fig. 6. Based on this way, the magnetic material could be fully utilized and the inductance value could be increased compared with single permeability inductor. However, it would be difficult to fabricate such a continuous changing permeability inductor in practice. Instead, we could divide the region of varying permeability into different small regions, and let each small region has a constant permeability. By doing this, a magnetic core whose permeability discretely changes could be realized. The inductors made with magnetic cores of this type are called multi-permeability inductors. Fig. 7 shows the structures of magnetic cores with discretely changing permeability.

$$\mu_r(l_r) = \frac{B_{\max} l_r}{\mu_0 I} \quad (2)$$

The length of magnetic path for circular cross-section magnetic core could be expressed by its circumference (3)

$$l_{r_circular} = 2\pi r \quad (3)$$

Where r is the radius of the circular magnetic path. And the per unit length inductance for a toroidal inductor could be thus expressed by (4)

$$L_{circular} = \int_{R_i}^{R_E} \frac{\mu_r(l_r) \mu_0}{l_{r_circular}} dr \quad (4)$$

Models for calculating inductance values of the planar inductors have been derived in [19]. The length of magnetic path could be expressed by the rounded corner rectangle. Its length of the magnetic path could be expressed by (5)

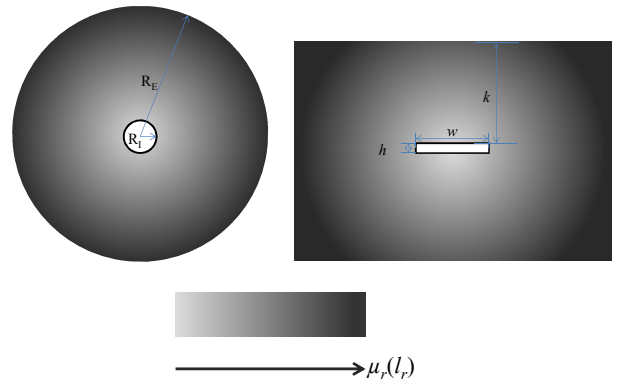


Figure 6. Continuous permeability distribution in distributed air gap inductors.

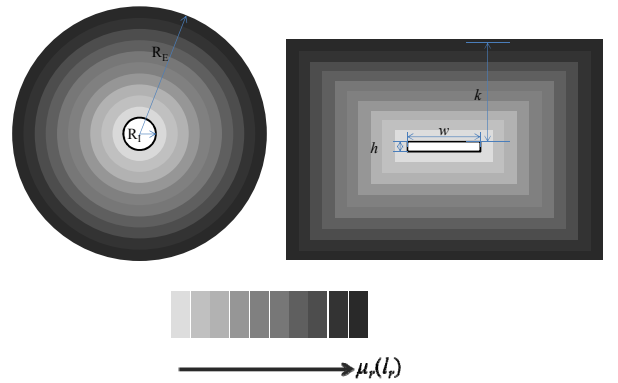


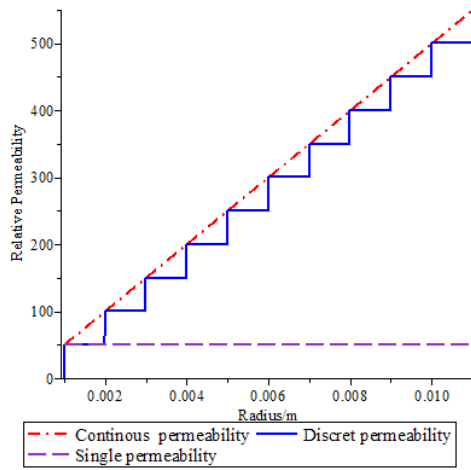
Figure 7. Discrete permeability distribution in distributed air gap inductor.

$$l_{r_square} = 2(w + h) + 2\pi r \quad (5)$$

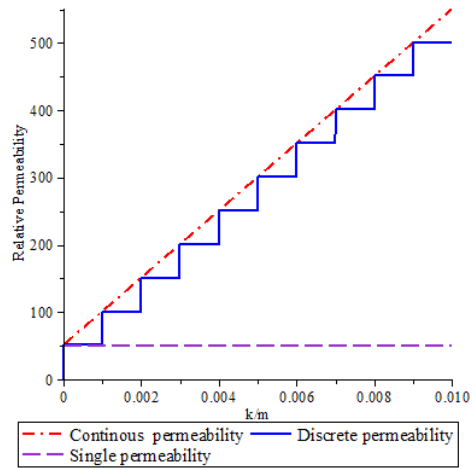
The per unit length inductance for a planar inductor could be expressed by (6)

$$L_{square} = \int_0^k \frac{\mu_r(l_r) \mu_0}{l_{r_square}} dr \quad (6)$$

Fig. 8 shows the permeability of inductors versus the radius and the height of the magnetic cores. Compared with low single permeability structure, the proposed magnetic cores have continuous or discretely increasing permeability with the increase of radius or height. This means much higher inductance values could be obtained while the volume remains unchanged. Per unit length inductance and the inductance density (obtained by dividing the inductance with inductor volume) of the same volume magnetic cores with the three kinds of permeability configurations are illustrated in Fig. 9 and Fig. 10. It can be observed that although the inductance of the multi-permeability inductor is a little bit less than that of the continuous changing permeability inductor, it is much higher than that of the single permeability inductor. And it also can be seen from Fig. 10 that the larger the radius or height is, the more significantly the inductance density increases.

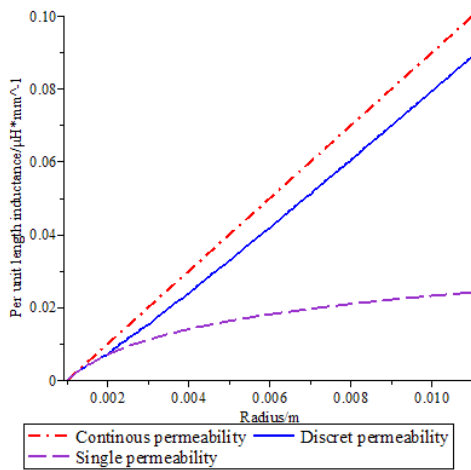


(a)

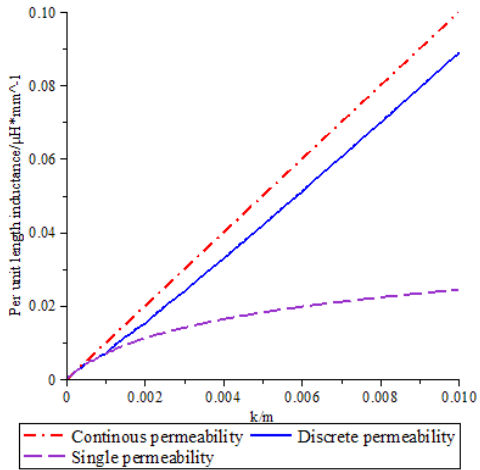


(b)

Figure 8. Permeability versus radius or height. (a) Circular cross-section magnetic core. (b) Square cross-section magnetic core.

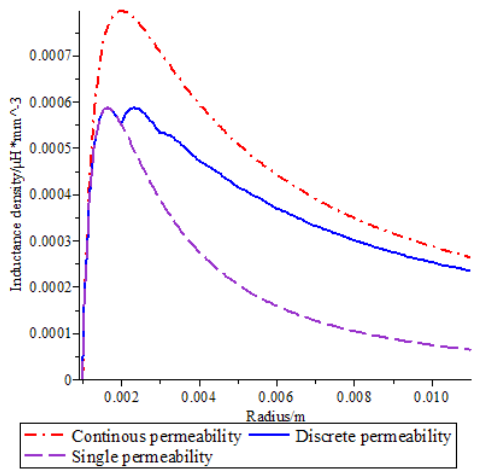


(a)

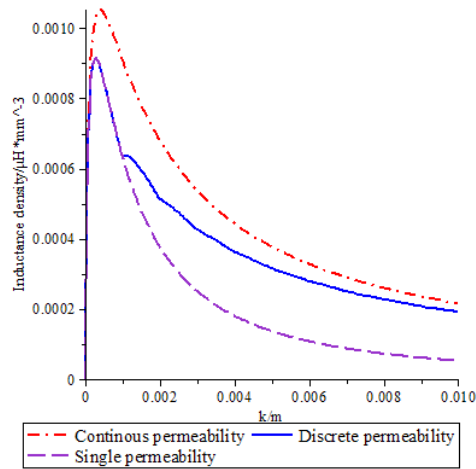


(b)

Figure 9. Per unit length inductance versus radius or height. (a) Circular cross-section magnetic core. (b) Square cross-section magnetic core.



(a)



(b)

Figure 10. Inductance density versus radius or height. (a) Circular cross-section magnetic core. (b) Square cross-section magnetic core.

A simulation is also set up to show the flux density distribution of multi-permeability inductors. The results are shown in Fig.11. Compared with single permeability magnetic cores in Fig. 5, the multi-permeability magnetic cores have much evenner high flux distribution, which make the whole cores fully utilized.

III. DESIGN OF A TWO-PERMEABILITY INDUCTOR

A. LTCC technology for realizing the inductor

Although the multi-permeability inductors have the advantage of increasing the inductance, it's difficult to make such magnetic cores with a conventional fabrication method. LTCC technology has been adopted in recent years to design some special magnetics for its advantage of three-dimensional integration [17]. In LTCC technology, the basic materials for fabrication are tapes including ceramic tapes, capacitor tapes and ferrite tapes. They could be co-fired together to realize passive integration if their temperature expansion coefficients (TEC) match each other well [21]. To fabricate a multi-permeability LTCC inductor, ferrite tapes of different permeability are laminated layer by layer to form a multi-layer structure and are co-fired in a furnace. Although the structure and flux density distribution are different from the inductors which were proposed in Section II, it could be used to approximately realize the same function. And for its irregular flux density distribution, finite element analysis (FEA) should be used for the design of such an inductor. In this paper, a two-permeability inductor prototype is designed to evaluate its performance. A single permeability inductor will also be designed for comparison.

B. Design of the LTCC inductors

Two kinds of ferrite tapes from ElectroScience (ESL) Corporation are selected to fabricate the inductors. They are 40010 [22] with relative permeability of 50 and 40011 [23] with relative permeability of 200. Unfortunately, the permeability of these two kinds of ferrite tapes are significant different, and there are no other available ferrite tapes whose permeability is between them. Therefore, to design a two-permeability inductor whose flux density distributes as fine as analyzed in Section II, the inner layer (40010) should be very thick so that the outer layer (40011) and inner layer (40012) could begin to saturate simultaneously. However, for the restriction of LTCC technology itself, it is difficult to design a thick planar inductor. For this reason, we only design a 2mm thick two-permeability inductor, and the high permeability ferrite tapes thus will firstly begin to saturate. This will inevitably discount the effect of increasing inductance especially at heavy load. But it should still be helpful at light load. And this problem could be easily solved when more ferrite tapes of lower permeability are available.

The perimeter of the conductor embedded in a LTCC inductor can be expressed by (7)

$$l = 2h + 2w \quad (7)$$

Where h is the thickness of the conductor; w is the width of the conductor.

The width of the conductor can be expressed by (8)

$$h = \frac{S}{w} \quad (8)$$

Where S is the area of the conductor. Substituting (8) into (7) results in (9)

$$l = 2w + \frac{2S}{w} \quad (9)$$

The total area of the conductor in this paper is set as a constant $S=0.8\text{mm}^2$, then by increasing w , the perimeter of the conductor will also increase correspondingly. Fig. 12 shows

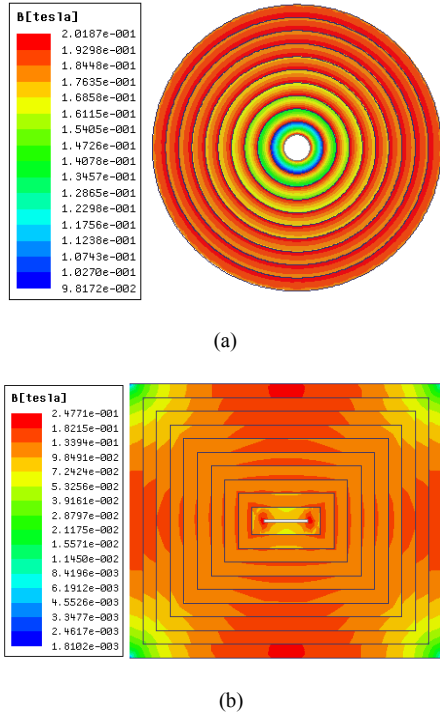


Figure 11. Flux density distribution of multi-permeability inductors. (a) Circular cross-section inductor. (b) Square cross-section inductor.

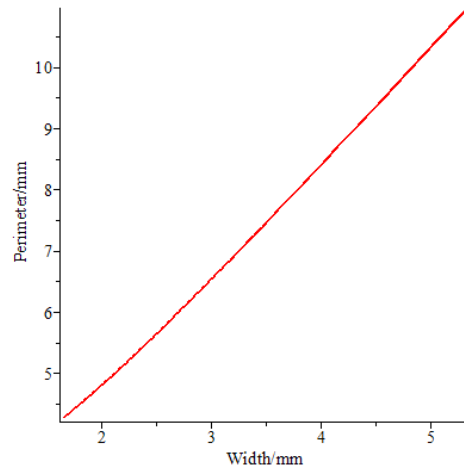


Figure 12. Perimeter versus width.

the relationship between the conductor perimeter and the conductor width for a single permeability inductor. With the increase of conductor width, the perimeter also rapidly increases. Correspondingly, the inductance rapidly reduces. Fig. 13 shows the per unit length inductance versus output current for a 2 mm thick single permeability inductor. The inductor whose conductor width is 5mm has the smallest light load inductance. With the decrease of conductor width, the light load inductance begins to increase, but the inductor is also subject to saturation at heavy load. It can be seen that for single permeability inductor, the light load inductance is too low when the conductor width is large ($w=5\text{mm}$). To increase the light load inductance, we may reduce the conductor width, however, the magnetic core is subject to saturation ($w=1\text{mm}$). In order to make an inductor with high current load capability and high light load inductance, a two-permeability inductor with wide conductor width could be designed. Fig. 14 shows the cross-section view of a two-permeability inductor. Fig. 15 illustrates per unit length inductance versus output current

with conductor width as a parameter ($h_m=1.2\text{mm}$, $h_c=0.4\text{mm}$). It can be seen that compared with single permeability inductor with the same conductor width, the two-permeability inductor has much higher light load inductance, which could help improve efficiencies of converters. To optimize the design of a two-permeability inductor, inductance values of different combination of h_m and h_c ($H=2\text{mm}$) are further simulated. Fig. 16 shows per unit length inductance versus output current for

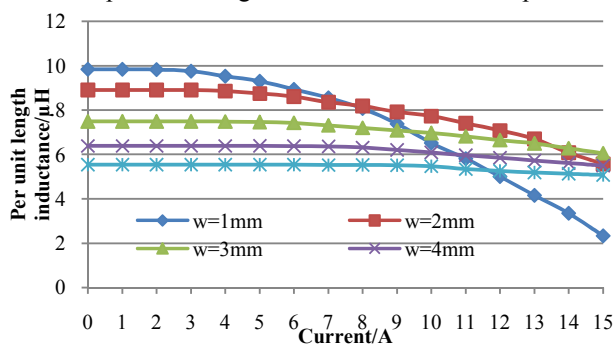


Figure 13. Per unit length inductance versus output current for single permeability inductors.

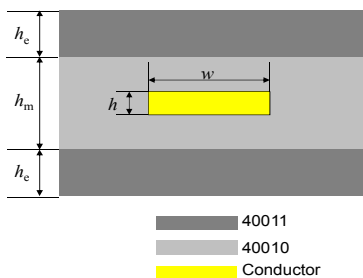


Figure 14. Cross-section view of a two-permeability inductor.

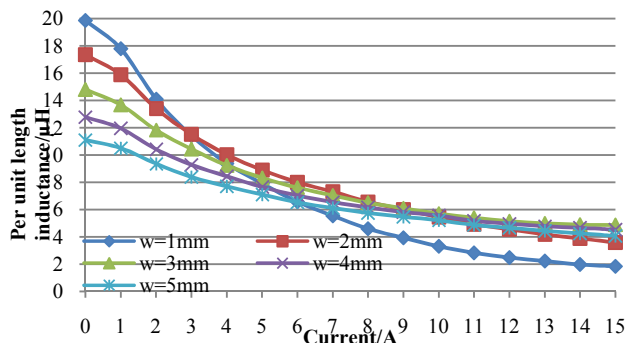


Figure 15. Per unit length inductance versus output current for two-permeability inductors.

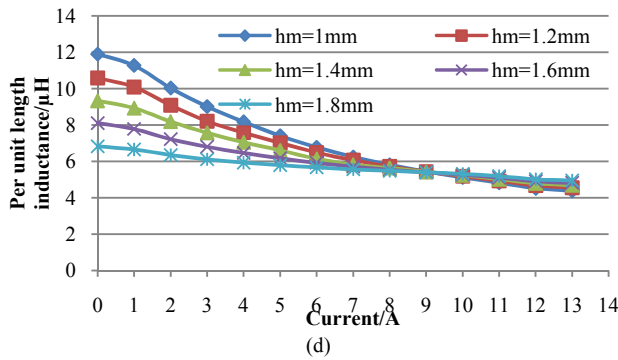
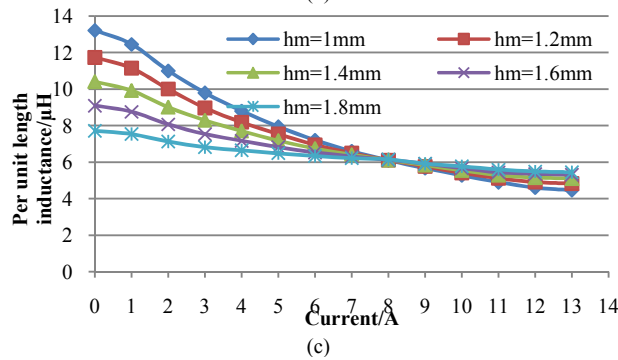
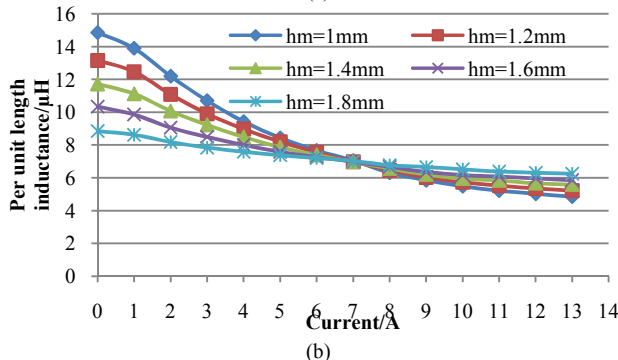
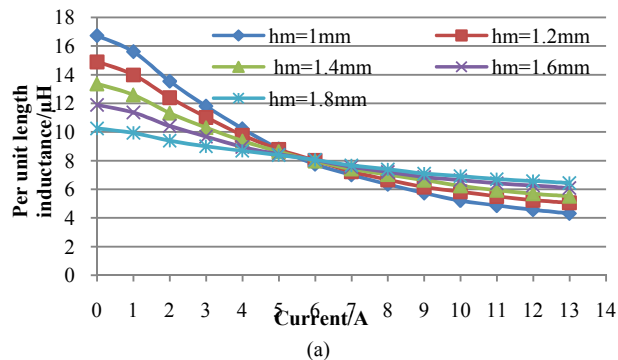


Figure 16. Per unit length inductance versus output current. (a) $w=2\text{mm}$. (b) $w=3\text{mm}$. (c) $w=4\text{mm}$. (d) $w=5\text{mm}$.

different width of conductor and thickness of ferrite tapes configurations. For certain conductor width, the thicker the high permeability ferrite tapes are, the higher the inductance is, however, after certain point of output current, the relationship is reversed. The thicker the high permeability ferrite tapes are, the lower the inductance is. The varying range of the inductance from light load to full load is highly related to width of the conductor. As a compromise of light load inductance and heavy load inductance, the conductor width of the inductor for fabrication is chosen to be 3mm and the thickness of low permeability ferrite is chosen to be 1.2m.

IV. FABRICATION AND EXPERIMENTS

A two-permeability inductor is fabricated to evaluate its performance. And for the purpose of comparison, a single permeability inductor of the same profile is also fabricated. Cross-section views of the two inductors are shown in Fig. 17. The single permeability inductor is made with 40010. The internal layer for the two-permeability inductor is 40010 while the outer layer is 40011. The fabrication process has been stated in detail in [12]. After lamination, the two inductors are put into a furnace and co-fired according to the temperature profile shown in Fig. 18. Fig. 19 shows the picture of the inductors. The inductance values versus current for the two inductors are shown in Fig. 20. To evaluate the light load efficiency performance of the two inductors, they are used in a 12V input, 1.6V output buck converter. The measured efficiencies are shown in Fig. 21. It can be observed that the converter has higher light load efficiency with the two-permeability inductor. However, because the outer layer ferrite tapes (40011) gradually become saturated, the inductance as well as the efficiency also gradually decreases at heavy load.

V. CONCLUSIONS

This paper proposed multi-permeability inductor structures to improve unevenly distributed flux density of distributed air-

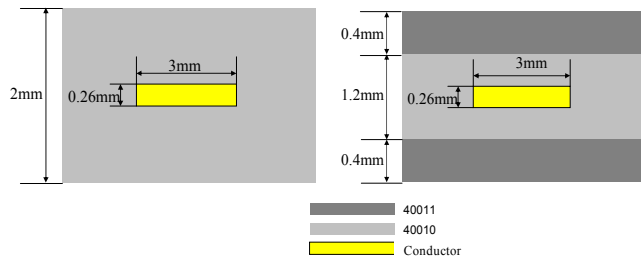


Figure 17. Dimensions of the single permeability and two-permeability inductors.

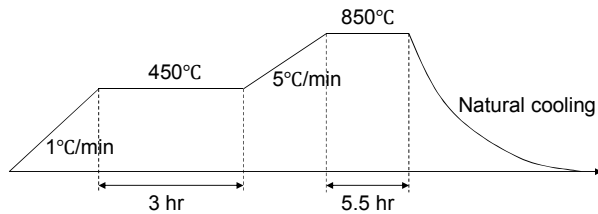


Figure 18. Temperature profile for co-firing.

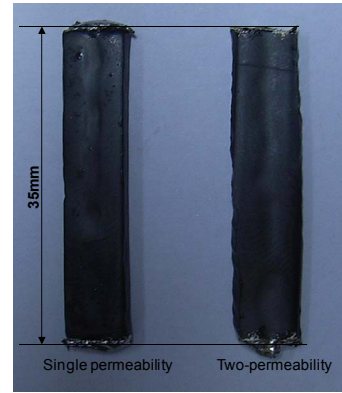


Figure 19. Prototypes of single permeability and two-permeability inductors.

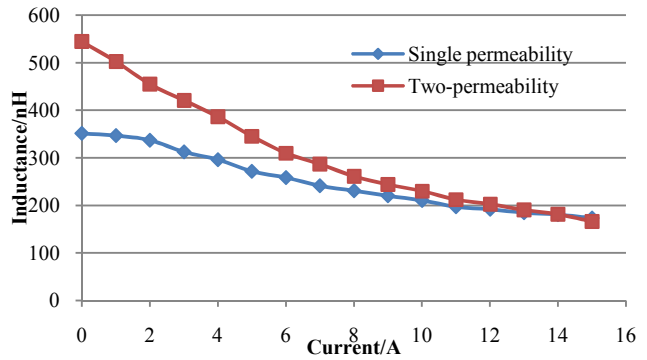


Figure 20. Per unit length inductance versus output current.

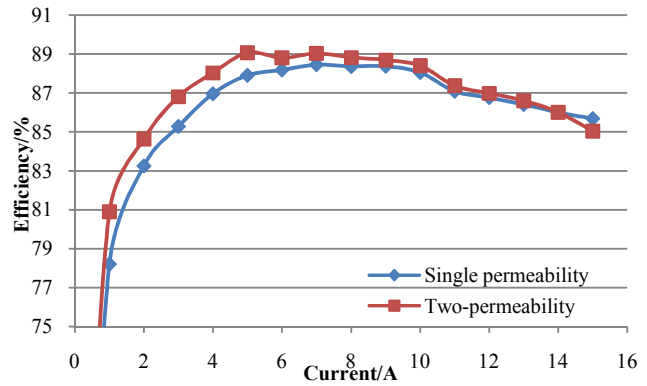


Figure 21. Efficiencies versus output current.

gap inductors, and based on the structures, inductance could be largely increased according theoretical analysis. Design of such an inductor is demonstrated with the aid of FEA simulation. Two prototypes of the same volume are fabricated based on LTCC technology, one is single permeability, and the other one is two-permeability. The experimental results show that the two-permeability inductor has higher inductance than the single permeability one at light load, and could improve light load efficiency of a DC/DC converter.

REFERENCES

- [1] Ngo, K. D. T. and M. H. Kuo. "Effects of air gaps on winding loss in high-frequency planar magnetics," in Proc. IEEE Power Electron. Spec. Conf., 1988. Vol.2, pp.1112-1119.
- [2] Chew, W. M., Evans, P. D. and Heffernan, W. J. "High frequency inductor design concepts," in Proc. IEEE Power Electron. Spec. Conf., 1991. pp.673-678.
- [3] Luca Daniel, Charles R. Sullivan and Seth R. Sanders "Design of microfabricated inductors," IEEE Trans. Power Electron., vol. 14, pp.709-723, Jul. 1999.
- [4] Jiankun, H. and C. R. Sullivan. "AC resistance of planar power inductors and the quasidistributed gap technique," IEEE Trans. Power Electron., vol 16, pp.558-567, 2001.
- [5] Jianing Wang, Xu Yang, Huapeng Niu, Zhaoan Wang, Jinjun Liu. "PCB integrated transformer composed with ferrite mosaics for LLC resonant converter," in Proc. IEEE Energy Conversion Congress and Exposition, 2009. pp.1032-1038.
- [6] E. Waffenschmidt, B. Ackermann, J. A. Ferreira, "Design Method and Material Technologies for Passives in Printed Circuit Board Embedded Circuits," IEEE Trans. Power Electron., vol. 20, no. 3, pp. 576-584, May. 2005.
- [7] Matthias Ludwig, Maeve Duffy, Terence O'Donnell, Paul McCloskey, and Seán Cian Ó Mathúna, "PCB Integrated Inductors for Low Power DC/DC Converter", IEEE Trans. Power Electron., vol. 18, no. 4, pp. 937-945, July. 2003.
- [8] C.-Y. Kim, H.-J. Kim, and J.-R. Kim, "An integrated LTCC inductor," IEEE Trans. Magn., vol. 41, pp. 3556-3558, 2005.
- [9] H.-J. Kim, Y.-J. Kim, and J.-R. Kim, "An Integrated LTCC Inductor Embedding NiZn Ferrite," IEEE Trans. Magn., vol. 42, pp. 2840-2842, 2006.
- [10] M. H. Lim, J.D. van Wyk, Zhenxian Liang, "Effect of geometry variation of LTCC distributed air-gap filter inductor on light load efficiency of DC-DC converters," in IEEE Industry Applications Conference, 2006, pp.1884-1890.
- [11] M. H. Lim, Zhenxian Liang, and J. D. van Wyk, "Low Profile Integratable Inductor Fabricated Based on LTCC Technology for Microprocessor Power Delivery Applications," IEEE Trans. Compon. Packag. Technol., vol. 30, pp. 170-177, 2007.
- [12] M. H. Lim, J. D. van Wyk, F. C. Lee, and K. D. T. Ngo, "A Class of Ceramic-Based Chip Inductors for Hybrid Integration in Power Supplies," IEEE Trans. Power Electron., vol. 23, pp. 1556-1564, 2008.
- [13] M. H. Lim, J. D. van Wyk, and F. C. Lee, "Hybrid Integration of a Low-Voltage, High-Current Power Supply Buck Converter With an LTCC Substrate Inductor," IEEE Trans. Power Electron., vol. 25, pp. 2287-2298, 2010.
- [14] Qiang Li, Yan Dong, F. C. Lee. "High density low profile coupled inductor design for integrated Point-of-Load converter," in proc. IEEE Applied Power Electronics Conference, 2010, pp.79-85.
- [15] Mingkai Mu, Yipeng Su, Qiang Li, F. C. Lee. "Magnetic characterization of low temperature co-fired ceramic (LTCC) ferrite materials for high frequency power converters," in Proc. IEEE Energy Conversion Congress and Exposition (ECCE), 2011, pp.2133-2138.
- [16] M. H. Lim, J. D. van Wyk, F. C. Lee. "Hybrid Integration of a Low-Voltage, High-Current Power Supply Buck Converter With an LTCC Substrate Inductor," IEEE Trans. Power Electron., vol. 25, pp.2287-2298, Sep. 2010.
- [17] Laili Wang, Yunqing Pei, Xu Yang, Xizhi Cui, and Zhaoan Wang, "Three-dimensional integration of high frequency DC/DC converters based on LTCC technology," in IEEE Power Electronics and Motion Control Conf., 2009., pp. 745-748.
- [18] Laili Wang, Yunqing Pei, Xu Yang, Zhaoan Wang, "Design of Ultrathin LTCC Coupled Inductors for Compact DC/DC Converters." IEEE Trans. Power Electron., vol. 26, pp.2528-2541, Sep. 2011.
- [19] Laili Wang, Yunqing Pei, Xu Yang, Xizhi Cui, Zhaoan Wang, Guopeng Zhao, "Design of multi-turn LTCC inductors for high frequency DC/DC converters," in proc. IEEE Applied Power Electronics Conference, 2010, pp.1610-1615.
- [20] Laili Wang, Yunqing Pei, Xu Yang, Qin Yang, and Zhaoan Wang. "Improving Light and Intermediate Load Efficiencies of Buck Converters with Planar Nonlinear Inductors and Variable On Time Control," IEEE Trans. Power Electron., in Press.
- [21] A. H. Feingold, M. Heinz, and R. L. Wahlers, "Compliant dielectric and magnetic materials for buried components," in Proc. IMAPS, 2002, vol. 4931, pp. 65-70.
- [22] NiZn ferrite tape 40010 datasheet. (2002)[Online].Available:http://www.electroscience.com/ceramic_tapes.html.
- [23] NiZn ferrite tape 40011 datasheet. (2002) [Online].Available:http://www.electroscience.com/ceramic_tapes.html.